frontiers | Frontiers in Marine Science

TYPE Original Research
PUBLISHED 26 May 2023
DOI 10.3389/fmars.2023.1169883

OPEN ACCESS

EDITED BY
Kyu-Jung Chae,
Korea Maritime and Ocean University, Republic of Korea

REVIEWED BY
Sudipta Rakshit,
Tennessee State University, United States
Hai-Lei Cao,
Fujian Agriculture and Forestry University, China

*CORRESPONDENCE
YongRui Pi
yrpi@outlook.com

RECEIVED 20 February 2023
ACCEPTED 05 May 2023
PUBLISHED 26 May 2023

CITATION
Tang Y, Jia W, Bao M, Qiu S, Pi YR, Liu C and Zhao J (2023) Pick-up of fluoroquinolones from the aqueous phase *via* magnetically propeled microrobots: kinetics, thermodynamics, and site energy distribution analysis. *Front. Mar. Sci.* 10:1169883. doi: 10.3389/fmars.2023.1169883

Pick-up of fluoroquinolones from the aqueous phase *via* magnetically propeled microrobots: kinetics, thermodynamics, and site energy distribution analysis

Yongzheng Tang[1], Wenpeng Jia[1], Mutai Bao[2,3], Shengyao Qiu[1], YongRui Pi[1]*, Chongfeng Liu[1] and Jinchen Zhao[1]

[1]School of Ocean, Yantai University, Yantai, China, [2]Frontiers Science Center for Deep Ocean Multispheres and Earth System, and Key Laboratory of Marine Chemistry Theory and Technology, Ministry of Education, Ocean University of China, Qingdao, China, [3]College of Chemistry and Chemical Engineering, Ocean University of China, Qingdao, China

Removing fluoroquinolones (FQs) in marine culture tailwater is crucial for the coastal marine environment. The application of a bacteria-based microrobot for FQ removal was discussed. Norfloxacin (NOR) and levofloxacin (LEV) had static maximum adsorption capacities of 114.8 and 49.4 mg/g, respectively, by a magnetic microrobot. The experimental results of NOR adsorption by a magnetic microrobot were well supported by the Langmuir isotherm and Elovich kinetic models. Both the Langmuir isotherm model and the pseudo-second-order kinetic model may be able to accurately represent the LEV adsorption process. The mass transfer mechanism of the NOR and LEV adsorptions was divided into two steps and described better using the intraparticle diffusion (IPD) model. The exothermic and spontaneity of the sorption process were demonstrated through the study of thermodynamics. The magnetic microrobot's heterogeneous surface was validated by the examination of site energy distribution. Additionally, this study demonstrated that the majority of the NOR and LEV sorption took place at sites with energies over 4.25 and 17.36 kJ/mol, respectively, supporting the notion that NOR and LEV adsorption constitute physical–chemical processes. Based on the above results, a magnetic microrobot, as a new-style green bio-adsorbent, can potentially be used to remove NOR and LEV from the mariculture in an inexpensive and effective manner.

KEYWORDS

magnetic microrobot, fluoroquinolones, kinetics, adsorption mechanisms, site energy distribution

1 Introduction

Fluoroquinolones (FQs) are extensively consumed for disease prevention and growth promotion in animal breeding and aquaculture (Coffie et al., 2021). Mariculture tailwater has drawn much attention, as it brings serious eutrophication offshore and damage to the surrounding estuary ecosystems (Gao et al., 2022). Also, some of the FQs were officially detected in the mariculture system around the world (Wang et al., 2022). Most of the FQs cannot be metabolized or absorbed by the body, and so enter into the environment instead (Oberoi et al., 2019). They have also been recognized as new toxic organic pollutants in the aquatic environment (Saya et al., 2022). Antibiotic residues in water may endanger the ecosystem and human health because they can cause central nervous system stimulation, convulsions, ocular problems, inhibition of the neurotransmitter gamma-aminobutyric acid, reproductive dysfunction, and gastrointestinal disturbances (Saya et al., 2022). It is imperative to develop a green and effective technology to remove antibiotic residues from the aquatic environment.

When FQs enter the environment, they undergo migration and transformation processes such as adsorption, hydrolysis, photolysis, and biodegradation (Sarmah et al., 2006; Patel et al., 2019; Yang et al., 2021). While FQs are relatively stable in water they are not particularly suitable for hydrolysis (Van Doorslaer et al., 2014; Patel et al., 2019). The photolysis process is much easier to carry out (Wammer et al., 2013; Lakshmi Prabavathi and Muthuraj, 2019), but will produce active free radicals and cause secondary pollution. Therefore, adsorption is the primary way of removing FQs in land-based mariculture tailwater since the biodegradation rate of FQs is very low (Oberoi et al., 2019; Saya et al., 2022). Many absorbents have been confirmed to remove FQs from aqueous media, such as clay minerals (Hacıosmanoglu ˘ et al., 2022), biochar (Cheng et al., 2021), activated carbon (Kah et al., 2017) and other carbonaceous materials (Scaria et al., 2022), plastic polymers (Rai et al., 2022), graphene-based nanomaterials (Wang et al., 2019a), and Fe-oxide-based composites (Chu et al., 2022). Some green materials, such as plant leaves, fruit, algae, fungi, and bacteria, were employed to achieve energy-efficient, cost-effective, and environmentally friendly removal of organic pollutants (Altaf et al., 2021). Moreover, the favored adsorption has some strengths, such as a simple operation process, high treatment efficiency, rich adsorbent materials, and no highly toxic by-products (Fang et al., 2021b; Hacıosmanoglu ˘ et al., 2022).

Magnetic substrate-loaded adsorbent has been employed in the removal of FQs with easy regeneration (Fang et al., 2021a). Magnetic micro/nanorobots have piqued the interest of researchers because of their enormous potential for use in biomedicine and environmental remediation (Zhou et al., 2021). In addition to their bio-friendliness, recoverability, and toxin-free nature due to magnetic manipulation, they can actively swim around aquatic contaminants and remove them *via* capture (adsorption/absorption) or degradation (Zhang et al., 2018). Owing to the strong dynamic intermixing, also known as the magnetic stirring function, the magnetic fields can also be used to speed up reaction kinetics or increase recognition efficiency. They can also be used to retrieve nano/microrobots after the cleaning process is finished (Ji et al., 2020). The magnetic micro/nanorobots will eventually be able to be recycled or reused without their parts being altered. To deal with oil spills, researchers designed a micromotor that moved like a walnut and was made of polycaprolactone, Fe3O4 nanoparticles, and catalase in a solution with H2O2. The micromotor could be navigated and recycled using an external magnetic field (Wang et al., 2019b). Porous biohybrid microrobots made of fungal spores and Fe_3O_4 nanoparticles were found to be very effective at removing heavy metal ions. The group behaviors and magnetically driven movement of the microrobots may enhance pollutant adsorption more than static microrobots (Zhang et al., 2018). Carbon soot-based micromotors were simultaneously activated by a magnetic field and oxygen microbubbles, allowing for efficient on-the-spot degradation of methyl blue (MB) dye contamination (Singh et al., 2020). Additionally, it has been reported that functional magnetic micromotors were powerful enough to absorb or remove antibiotics from contaminated water (Li et al., 2019b; Liu et al., 2019).

In a previous study, we made magnetic microrobots with iron (II, III) oxide nanoparticles (Fe_3O_4 NPs) based on hydrocarbon-degrading bacteria (Pi et al., 2022). The magnetic microrobot performed excellently for Congo red adsorption from the aquatic phase (Pi et al., 2022). Owing to FQs having a similar benzene ring structure to that of organic dye, the removal of FQs with the help of a magnetic microrobot was the goal of this work. Norfloxacin (NOR) and levofloxacin (LEV) are FQs that are used widely, and the concentration of ng/L to μg/L has been detected in different aqueous environments (Fang et al., 2021a, b; Yan et al., 2017a; Yan et al., 2017b). They were used as typical FQs in this work. Adsorption capacity, kinetics, isotherm equilibrium, site energy distribution analysis, and mechanism were used to investigate NOR's and LEV's removal potential. Adsorption parameters, which corresponded to a specific site energy distribution, were also determined using a variety of isotherm models. Owing to their magnetic characteristics, microrobots were easy to navigate and were recycled under a magnetic field.

2 Materials and methods

2.1 Materials

Without further purification, all chemicals are at an analytical grade. The bacteria were isolated from an antibiotic-producing pharmaceutical factory's sewage outlet. Our previous research serves as a reference for the isolation procedure (Pi et al., 2015).

2.2 Synthesis of microrobots

The microrobot can be simply defined as a nanocluster magnetite (Fe_3O_4) attached to bacteria. The Fe_3O_4 was prepared

in accordance with previous studies (Schwertmann and Cornell, 2000; Jiang et al., 2018; Jiang et al., 2020). The preparation of magnetic microrobots is referred to in the literature (Pi et al., 2022; Vaghasiya et al., 2022). The details of the characterization of bio-based materials were also demonstrated according to the field emission scanning electron microscopy (FESEM), transmission electron microscopy (TEM), fourier transform infrared (FTIR), and X-ray diffraction (XRD), nitrogen adsorption-desorption isotherms, magnetic behaviors, and point of zero charges (Pi et al., 2022).

2.3 Adsorption experiments

All adsorption experiments were conducted using 50-mL glass tubes in accordance with our previous work (Wang et al., 2021; Pi et al., 2022). To investigate the adsorption isotherm equilibrium, 50.0 mL of a NOR/LEV solution was mixed with 5 mg Fe_3O_4 or a magnetic microrobot, with initial NOR/LEV concentrations ranging from 10 to 50 mg/L. In addition, 0.1 mol/L NaOH and/or 0.1 mol/L HCl solutions were used to adjust the NOR/LEV solutions' pH. The tubes were shaken at 150 rpm at a controlled temperature using a shaker in the dark. Then, the pH value (4–10), the adsorbent dose, and the adsorption temperature were changed to obtain the adsorption capacity.

In the kinetics experiments, a 500-mL NOR/LEV solution was mixed with moderate adsorbents. The NOR/LEV solution was measured using high-performance liquid chromatography (HPLC) after being adsorbed for various amounts of time. To avoid light, all samples were shaken in the dark. Each experiment was replicated three times.

Ultraviolet-(UV-)HPLC (1260, Agilent Technologies) was utilized for the detection of NOR and LEV. With a mobile phase of 60:40 (v/v) acetonitrile anhydrous and formic acid at 1% in deionized water and a flow rate of 0.75 mL/min, the HPLC was equipped with a C18 column (2.7 m, 4.6 mm × 100 mm). The wavelengths used for UV detection were 278 nm (NOR) and 293 nm (LEV).

2.4 Methods of data analysis

2.4.1 Equilibrium adsorption capacity

The following formulae (1–3) were used to calculate the NOR/LEV removal efficiency (adsorption percentage), adsorption capacities at time t, and equilibrium:

$$R = \frac{(C_0 - C_e)}{C_0} \times 100 \quad (1)$$

$$q_t = \frac{(C_0 - C_t)}{w} V \quad (2)$$

$$q_e = \frac{(C_0 - C_t)}{w} V \quad , \quad (3)$$

where R is the NOR/LEV's removal efficiency; C_0 (mg/L), C_e (mg/L), and C_t (mg/L) are the concentrations of the initial, equilibrium, and time t of the NOR/LEV, respectively; the NOR/LEV's adsorption capacities at time t and equilibrium are q_t (mg/g) and q_e (mg/g); and the adsorbent's mass is w (g) and V (L) is the volume of the solution (Pi et al., 2022).

2.4.2 Fitting of adsorption isotherms

The empirical relationships between adsorption capacities of NOR/LEV on Fe_3O_4 and the magnetic microrobots with the equilibrium concentration in the liquid phase were fitted with Langmuir, Freundlich, Temkin (Pi et al., 2022), and Langmuir–Freundlich (Yan et al., 2017a; Yan et al., 2017b) isotherm (Carter et al., 1995) equations (4–7):

$$\frac{C_e}{q_e} = \frac{C_e}{q_m} + \frac{1}{K_L q_m} \quad (4)$$

$$\ln q_e = \ln K_F + \frac{1}{n_F} \ln C_e \quad (5)$$

$$q_e = \left(\frac{RT}{b_T}\right) \ln (K_T C_e) \quad (6)$$

$$q_e = \frac{q_m b C_e^n}{1 + b C_e^n} \quad , \quad (7)$$

where K_L (L/mg), K_F [(mg/g) (L/mg)$^{1/n}$], and K_T (L/mg) are the adsorption coefficients for the Langmuir, Freundlich, and Temkin models, respectively. q_m (mg/g) was the calculated maximum value of the adsorbents' NOR/LEV adsorption capacity. The $1/n_F$ indicates the Freundlich model parameter, while b_T (L/mg) is the equilibrium constant for the adsorption of the Temkin model (Yan et al., 2017a; Yan et al., 2017b). b (L/mg) is the equilibrium constant for the adsorption of the Langmuir–Freundlich model.

2.4.3 Fitting of adsorption kinetics

The pseudo-first-order, pseudo-second-order, and Elovich kinetic models were used to establish the rate-governing adsorption process, as shown below (8–10) (Sun et al., 2022):

$$\ln (q_e - q_t) = \ln q_e - k_1 t \quad (8)$$

$$\frac{t}{q_t} = \frac{1}{k_2 q_e^2} + \frac{t}{q_e} \quad (9)$$

$$q_t = \alpha + \beta \ln t \quad , \quad (10)$$

where k_1 (h^{-1}) and k_2 (g/mg·h) are the pseudo-first-order and pseudo-second-order rate constants, respectively. In the Elovich model, α and β are constants.

2.4.4 Mass transfer mechanisms

The adsorption process's speed-limiting steps were investigated using intraparticle diffusion (IPD) (Wang et al., 2010) and liquid film diffusion (LFD) models.

The LFD and IPD models were expressed as:

$$-\ln (1 - F) = k_3 t \quad (11)$$

$$q_t = k_{IPD} t^{1/2} + c \quad (12)$$

The constant for the diffusion rate of a liquid film is k_3 (min^{-1}), and F is the q_t/q_e. The IPD diffusion rate constant is k_{IPD} [mg/(g·$min^{1/2}$)], and the linear intercept c (mg/g) provides information about the thickness of the boundary layer (Foroutan et al., 2021).

2.4.5 Thermodynamic calculation

The following equations were used to calculate the thermodynamic parameters to ascertain the nature of the adsorption process (13–15):

$$K_c = \frac{q_e}{C_e} \quad (13)$$

$$\ln K_c = \frac{\Delta S}{R} - \frac{\Delta H}{RT} \quad (14)$$

$$\Delta G = -RT \ln K_c \quad , \quad (15)$$

where the coefficient of the adsorption distribution is K_c (L/g). Entropy, enthalpy, and Gibb's free energy are represented by ΔS (J/mol), ΔH (J/mol), and ΔG (J/mol·K), respectively. The universal gas constant is R (8.314 J/mol K) and the temperature is T (K).

2.4.6 Approximate site energy distribution

The adsorbent's adsorption site energy distribution was linked to the equilibrium adsorption capacity (Carter et al., 1995). Using the parameters of the Langmuir–Freundlich model, the following equations (16,17) were used to determine the magnetic microrobot's site energy distribution:

$$E* = E - E_s = RT \ln \left(\frac{C_s}{C_e}\right) \quad (16)$$

$$F(E*) = \frac{q_m n b C_s^n}{RT} \bullet \frac{e^{-nE*/RT}}{(1 + bC_s^n e^{-nE*/RT})^2} \quad (17)$$

where $C_e = C_s$, E_s is the adsorption energy, E^* is the difference in adsorption energies between the adsorbate and solvent on the adsorbent surfaces, and $F(E^*)$ is an approximate site energy distribution function. The adsorbate's maximum solubility is C_s (mg/L). The C_s value of NOR in water is 303.5mg/L, 400 mg/L, 522.1 mg/L, 678.2 mg/L, and 872.5 mg/L at 293.15 K, 298.15 K, 303.15 K, 308.15 K, and 313.15 K (pH=7), respectively (Ross and Riley, 1990; Blokhina et al., 2016). The C_s value of LEV in water is 46, 50, 54, 58, and 62 mg/mL at 293.15, 298.15, 303.15, 308.15, and 313.15 K, respectively (Ross and Riley, 1990; Blokhina et al., 2016).

The adsorption site energy distribution, which can be calculated using the following equation, was used to determine the average site energy:

$$u(E*) = \frac{\int_0^\infty E*F(E*)d(E*)}{\int_0^\infty F(E*)d(E*)} \quad (18)$$

Incorporating the above equation with Eq. (16) and Eq. (17), the average site energy could be determined as follows:

$$\mu(E*) = \frac{RT}{n} \ln (1 + bC_s^n) \quad (19)$$

3 Results and discussion

3.1 Adsorption property for norfloxacin and levofloxacin

3.1.1 Effect of initial norfloxacin and levofloxacin concentration

The impact of the initial concentrations of NOR and LEV on the relative adsorption capacity and removal efficiency on the magnetic microrobot is illustrated in Figures 1A, B. The relative adsorption capacity increased with the initial concentration until 40 and 50 mg/L for NOR and LEV, respectively. The concentration gradient is a vital driving force between the liquid adsorbate and solid adsorbent. When it overwhelmed the resistance to bulk transfer between the adsorbate and adsorbent, the adsorption was enhanced as if the initial concentration of the adsorbate had increased (Altaf et al., 2021). Also, the limited adsorption site of the adsorbent reached a saturation state with the increase of the initial concentration. Thereafter at this point, the absorbent achieved the equilibrium, with the adsorption capacity up to 63.8 and 49.4 mg/g for NOR and LEV, respectively. The removal efficiency of NOR and LEV decreased gradually with the increase of the initial concentration. This can be attributed to the fixed amount of adsorbent dosage in this experiment.

3.1.2 Effects of adsorbent dosage

The effect of the adsorbent dose on the adsorption capacity and removal efficiency is presented in Figures 1C, D. When the dosage increased from 3 to 30 mg, the removal efficiency increased significantly due to the increase in the number and surface area of the active adsorption sites (Altaf et al., 2021; Fang et al., 2021). Also, the aggregation of the adsorbents resulting from a high dose of nanoparticles enhanced the removal efficiency (Altaf et al., 2021), while aggregation led to a decrease in the total surface area of the adsorbent (Fang et al., 2021b). The adsorption capacity increased with the increasing dosage, from 3 to 5 mg, peaking at 5 mg. The high adsorption capacity at 5 mg could be attributed to the fulfillment of most binding sites and an increase in total surface area (Zhou et al., 2018). Then, there was a decline when the adsorbent dosage was larger than 5 mg, indicating that the absorbent achieved equilibrium. While the capacity was calculated using the relative adsorption dose, the value declined according to the increased dose of the adsorbent.

3.1.3 Effect of pH

The pH of the solution, which plays a crucial role in the adsorption process, can alter the adsorbents' surface charges and adsorbate ionization, affecting the adsorption capacity even more (Fang et al., 2021a). Because they have two distinct acid dissociation (pKa1 and pKa2) from the carboxyl group and the amino group, respectively, the form and adsorption effects of NOR and LEV were

10.3389/fmars.2023.1169883

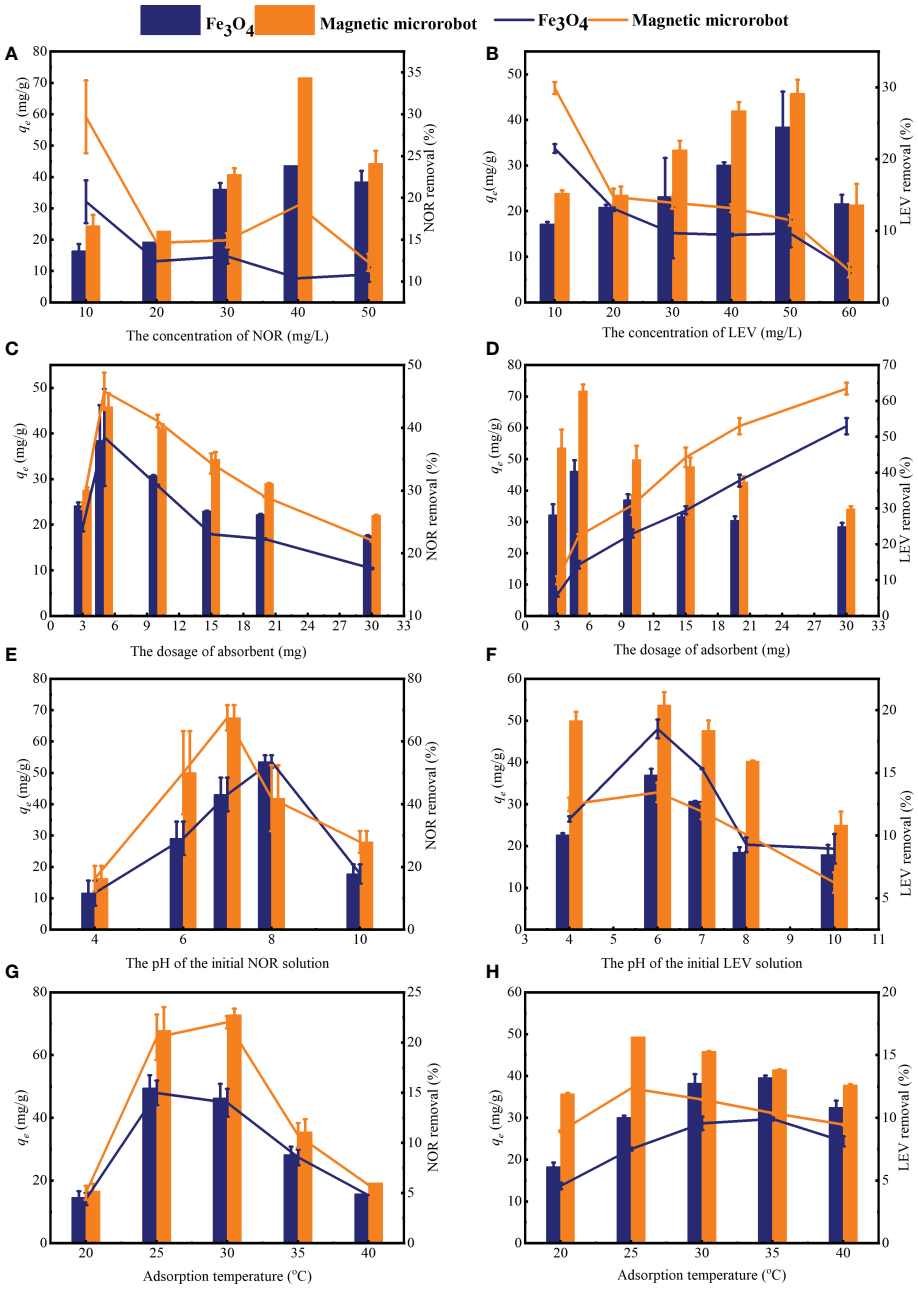

FIGURE 1
The adsorption properties and removal percentage of norfloxacin (NOR) and levofloxacin (LEV) on Fe_3O_4 and the magnetic microrobot. **(A, B)** The initial concentrations of NOR and LEV, **(C, D)** the adsorbent dosages, **(E, F)** the initial pH of NOR and LEV, and **(G, H)** the adsorption temperature. Note: the columns represent the adsorption capacity and the lines represent the removal efficiency.

determined by the pH value of the solution, as shown in Figure 2. If the solution pH was< pK_{a1}, -COOH and -NH_2^+- existed in the molecular of the cationic form. When the solution pH was > pK_{a2}, -COO^- and -NH- existed in the molecular in anionic form. When $pK_{a1<}$ pH< pK_{a2}, then NOR and LEV were in the zwitterionic form with -COO^- and -NH_2^+- existed in the molecular form.

Figures 1E, F depict the adsorption capacity and removal efficiency onto a magnetic microrobot at various initial pH levels, from 4 to 10. It can be seen that the adsorption limit and expulsion proficiency under similar circumstances were NOR > LEV. The adsorption capacity and removal efficiency of the capacity increased with the pH ranging from 4 to 7 for NOR, peaking at pH = 7. The LEV adsorption had a similar trend to that of NOR, with the highest adsorption capacity at pH = 6. The removal capacities were 63.8 and 49.2 mg/g, respectively. The adsorption capacity and removal efficiency significantly declined as the pH increased from 7 to 10. In general, the adsorbents' uptake of FQs was higher under $pK_{a1<}$ pH< pK_{a2} than acid or alkaline conditions, which was related to the properties of the FQs in zwitterionic form. The results are consistent with the studies conducted by Altaf et al. (2021). The adsorption capacity reached its maximum value at a pH of approximately 7, which is consistent with the structural characteristics of zwitterionic

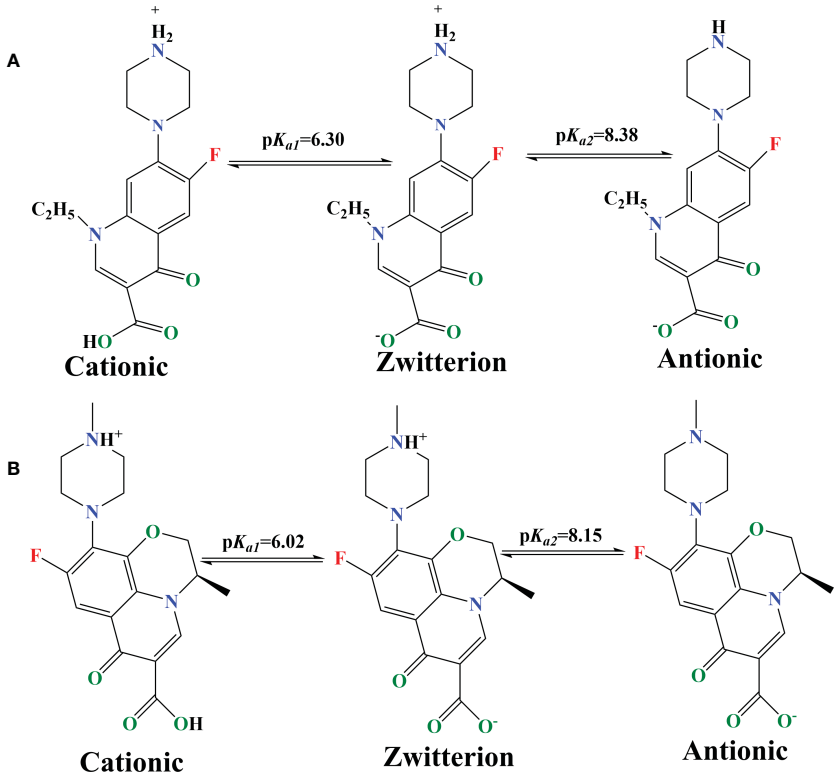

FIGURE 2
Molecular structure and pH-dependent speciation of **(A)** NOR (norfloxacin) and **(B)** LEV (levofloxacin).

FQs (Yan and Niu, 2017; Yan and Niu, 2018), and the quantity of zwitterionic FQs gradually increased with pH, implying that FQ adsorption results from complementary ion–pair interactions (Jiang et al., 2021). According to the research, Fe_3O_4 makes a passive oxide layer by coating on the surface when the pH is > 7 and reduces the FQ adsorption from the magnetic microrobot (Rezaei and Vione, 2018).

3.1.4 Effect of temperature

The adsorption performances of NOR and LEV by magnetic microrobot at various temperatures are presented in Figures 1G, H, respectively. The highest adsorption capacity and removal efficiency were achieved at 30°C for NOR and at 25°C for LEV. The interaction between FQs and absorbents was enhanced due to the active site expansion, when the adsorption temperature increased from 20°C to 30°C for NOR and 25°C for LEV (Altaf et al., 2021). While the adsorption temperature continued rising, the updraft movement of FQs was enhanced, which weakened the attraction between active adsorption sites and themselves, leading to the decline of the adsorption capacity and removing efficiency (Chen et al., 2011).

3.2 Adsorption isotherms

The experimental data and model-fitted findings for NOR and LEV adsorption from a magnetic microrobot are shown in Table 1. The non-linearity of the NOR and LEV adsorption isotherms on the absorbents suggests that the NOR and LEV concentrations and distributional effects were related to the magnetic microrobot's adsorption capacity (Sun et al., 2022). At various temperatures, the R^2 values of the Langmuir isotherm model were greater than those of the Freundlich, Temkin, and Langmuir–Freundlich isotherm models, indicating that NOR and LEV mostly adsorb onto the absorbents in monolayers. In the Freundlich model, n_F is the parameter relating to the mean energy of adsorption. If n_F> 1, it is preferred that adsorption is chemisorption in nature, and a strong adsorbent/adsorbate interaction occurs (Lv et al., 2020; Gaho et al., 2022). The calculated values of n_F were all larger than 1, indicating the chemisorption of NOR and LEV on the absorbents.

Many different adsorbents were listed in the comparison of the adsorption capacity with magnetic microrobots. As shown in Table 2, the Q_m for NOR was 698.6 mg/g by FRMB consisting of SDS (Li et al., 2019a). The $Q_m$of Fe_3O_4-based adsorbents (5-IOW and 14-IOW) for NOR (8.64 and 6.48 mg/g) were significantly lower than those of the magnetic microrobot. The $Q_{m,exp}$ of the magnetic microrobot for NOR was much larger than for most other adsorbents (Table 2). The Q_m for LEV was 298.43 mg/g by PCS-KOH (Yang et al., 2020), which was much higher than for the other absorbents. The $Q_m$of the Fe_3O_4-based adsorbent (Fe_3O_4-gINPs) for LEV was 22.47 mg/g, which was much lower than that of the magnetic microrobot. Compared with other adsorbents, a magnetic microrobot can be used as one of the markedly superior adsorbent materials in wastewater treatment containing NOR or LEV.

TABLE 1 Adsorption equilibrium isotherm models on norfloxacin (NOR) and levofloxacin (LEV) using a magnetic microrobot.

Isotherm model	Model parameters	NOR					LEV				
		293.15K	298.15K	303.15K	308.15K	313.15K	293.15K	298.15K	303.15K	308.15K	313.15K
	$q_{m,\ exp}$(mg/g)	36.68	60.26	55.02	25.33	21.84	35.72	49.36	45.86	41.48	37.83
Langmuir $\frac{C_e}{q_e}=\frac{C_e}{q_m}+\frac{1}{K_L q_m}$	$q_{m,cal}$(mg/g)	73.53	153.61	62.46	31.76	23.66	2.337	113.51	359.71	94.70	165.84
	K_L (L/mg)	$2.39*10^{-4}$	0.01618	0.0545	0.04095	0.07788	0.01424	0.009694	0.003193	0.01636	0.006584
	$R2$	0.9842	0.9888	0.8502	0.4715	0.7532	0.8375	0.7276	0.9674	0.9739	0.9840
Freundlich $\ln q_e=\ln K_F+\frac{1}{n_F}\ln C_e$	K_f ((mg/g)(L/mg)$^{1/n}$)	0.52	3.778	5.987	1.609	2.847	2.074	1.306	1.229	19.06	1.652
	n_F	0.9317	1.322	1.804	1.289	1.805	1.484	1.143	1.049	1.452	1.216
	$R2$	0.9582	0.9517	0.7958	0.8263	0.9985	0.6660	0.6765	0.9724	0.9644	0.9781
Temkin $q_e=(\frac{RT}{b_T})\ln(K_T C_e)$	b_T (J/mol)	141.28	95.06	143.98	225.78	325.69	167.42	97.40	86.78	125.62	122.10
	K_T (L/mg)	0.1257	0.2346	0.3454	0.2431	0.3707	0.1471	0.09889	0.1043	0.1577	0.1251
	$R2$	0.7809	0.9226	0.6449	0.8891	0.9852	0.5128	0.5452	0.9319	0.9414	0.9807
Langmuir–Freundlich $q_e=\frac{q_m b C_e^n}{1+bC_e^n}$	q_m(mg/g)	20475.1	3660.9	30416.6	2221.49	48.87	12782.3	40599.3	2184.9	1361.5	93.14
	b(L/mg)	$9.47*10^{-6}$	$7.37*10^{-4}$	$8.43*10^{-5}$	$4.22*10^{-4}$	0.0457	$3.78*10^{-5}$	$4.55*10^{-6}$	$4.87*10^{-4}$	0.0021	0.0088
	n	1.3545	0.8870	0.8466	0.8458	0.7614	1.1117	1.4427	0.9997	0.7064	1.1383
	R^2	0.9358	0.9963	0.7264	0.8242	0.9898	0.7823	0.2015	0.9557	0.9154	0.9653

10.3389/fmars.2023.1169883

TABLE 2 Comparison of the adsorption capacities of different adsorbents for the removal of norfloxacin (NOR) and levofloxacin (LEV) at ambient temperatures (25°C).

Adsorbent	NOR		Adsorbent	LEV	
	$Q_{m,exp}$ (mg/g)	Reference		$Q_{m,exp}$ (mg/g)	Reference
γ-Fe_2O_3@BC	5.52	Wang et al., 2020	Fe-P-Mt	48.61	Liu et al., 2015
SCGB	19.52	Nguyen et al., 2022	Humic acid-treated zeolite	35.45(pH=4.85)	Chen et al., 2019
5-IOW	8.64	Fang et al., 2021b	47.68(pH=9.44)		
14-IOW	6.48		G.Zn/MCM	60.5	Abukhadra et al., 2022
HLB	529.85	Zhou et al., 2023	PCS-900	299.23	Yang et al., 2020
FRMB	299.6	Li et al., 2019a	PCS-KOH	298.43	
FRMB/SDS	698.6		PCS-Na_2CO_3	279.47	
FRMB/SDBS	589.9		PCS-700	259.61	
ZIF-8	63.29 (293K)	Zhou et al., 2019	AC	247.09	
	66.82 (303K)		MWCNT	116.09	
	69.44 (313K)		BC	76	Xu et al., 2021
PDMPs	304 (298K)	Wan et al., 2018	NFBC	172	
	321 (308K)		Fe_3O_4–gINPs	22.47	Altaf et al., 2021
	332 (318K)		BMF	115	Yao et al., 2021
magnetic microrobot	114.8	This work	magnetic microrobot	49.4	This work

3.3 Adsorption kinetics

The kinetic data of NOR and LEV fitted with three kinetic models are presented in Figure 3 and Table 3. Based on Figure 3 and the high R^2 values in Table 3, the adsorption of NOR fitted the Elovich kinetic model well, while the adsorption of LEV fitted the pseudo-second-order model well. The Elovich model was suitable for simulating the adsorption of NOR, showing that it is the valence electron, rather than just the electrostatic attraction, that causes the adsorption of NOR on to magnetic microrobots (Sun et al., 2022). The main process involved in LEV kinetic adsorption was chemisorption due to the pseudo-second-order model (Sun et al., 2022).

3.4 Mass transfer mechanisms

According to temperature, pressure, and the types of adsorbent and adsorbate, varied mass transfer resistances may be able to limit the adsorption rate, which was evaluated using a kinetic analysis. The solid material was characterized by two primary resistances: protection from outer dissemination (interparticle), connected with mass exchange from mass liquid to the outside surface, and intraparticle dispersion, connected with mass exchange from an outside surface to an internal permeable construction. To investigate mechanisms and the potential rate-determining steps, several models have been proposed. Piecewise and linear regressions were used to fit the adsorption data using the IPD and LFD models to investigate the specific adsorption processes of NOR and LEV. The results are shown in Figure 4 and Table 4. The IPD model was better suited to represent the mass transfer process of NOR and LEV adsorption by Fe_3O_4 and a magnetic microrobot based on the statistical parameter ($R^2 > 0.90$). From Figures 4A, B, the fact that the connection between q_t and $t^{1/2}$ is non-linear and does not pass through the origin point indicates that there are other rate-limiting steps besides IPD and that the rate of adsorption may potentially be controlled by an external diffusion mechanism. IPD and equilibrium are the two steps of the adsorption process. The adsorption rate of NOR and LEV was $k_{IPD1} > k_{IPD2}$. The first stage was relatively slow, and the second stage represented the equilibrium condition for the adsorption–desorption process. The internal mass transfer restriction of the magnetic microrobot was stronger than that of Fe_3O_4 based on the fact that the R^2 of the magnetic microrobot for NOR adsorption was higher than that of Fe_3O_4 (Yu et al., 2021). In conclusion, NOR and LEV were adsorbed on magnetic microrobots by a chemical process that was regulated simultaneously by internal and exterior diffusion processes.

3.5 Adsorption thermodynamics

To examine the adsorption thermodynamics of NOR and LEV on a magnetic microrobot, a range of temperatures, including 298, 303, 308, 313, and 318 K were chosen. It is clear from Table 5 that the adsorption of NOR had a negative ΔH value, which indicates that the process was exothermic and involved the adsorption of both chemical and physical substances. LEV adsorption by the magnetic microrobot was an endothermic process (ΔH>0), which

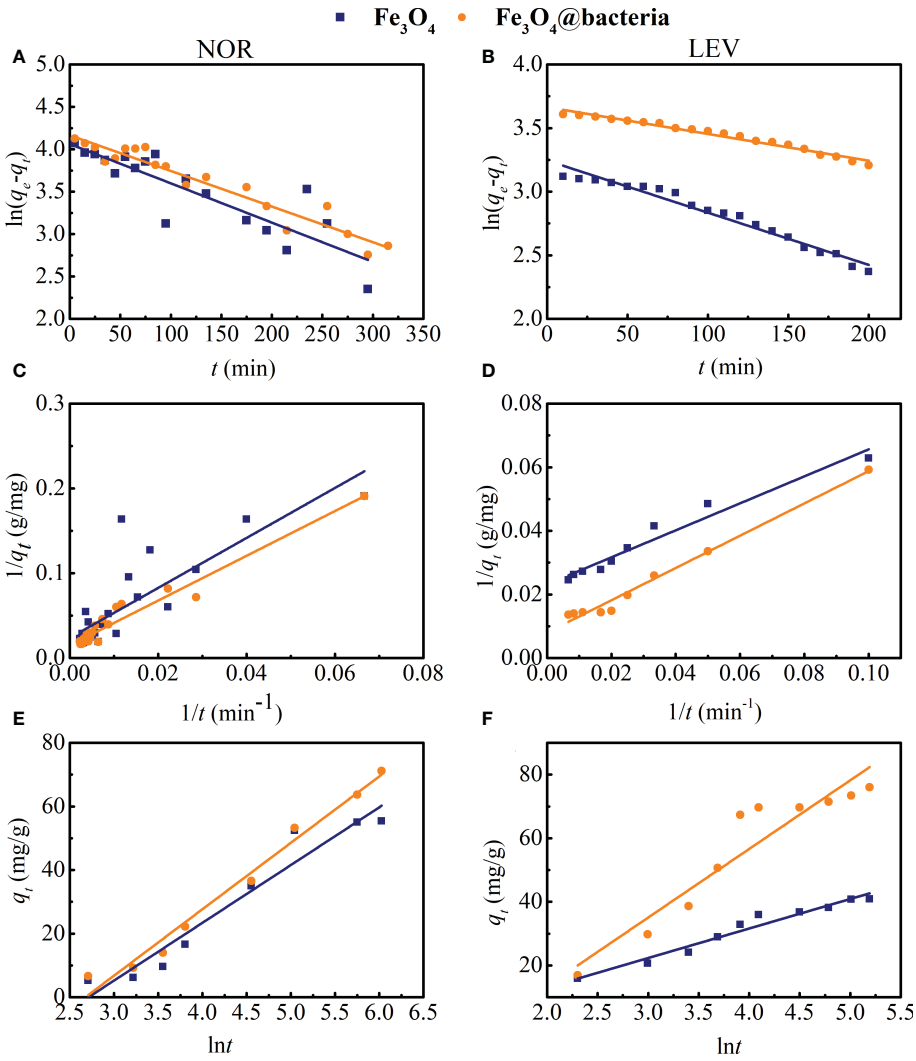

FIGURE 3
(A, B) Pseudo-first-order kinetic model, **(C ,D)** Pseudo-second-order kinetic model, and **(E, F)** Elovich kinetic model for norfloxacin (NOR) and levofloxacin (LEV) adsorption.

TABLE 3 Adsorption kinetic models on norfloxacin (NOR) and levofloxacin (LEV) using Fe_3O_4 and a magnetic microrobot.

Kinetic model*	Parameters	NOR		LEV	
		Fe_3O_4	magnetic microrobot	Fe_3O_4	magnetic microrobot
	$q_{e,exp}$(mg/g)	57.16	61.14	38.47	53.78
PFO $\ln(q_e - q_t) = lnq_e - k_1 t$	$q_{e,cal}$(mg/g)	58.08	64.39	25.66	39.03
	$k_1(h^{-1})$	0.00463	0.0042	0.0041	0.0021
	R^2	0.7374	0.9237	0.9662	0.9732
PSO $\frac{t}{q_t} = \frac{1}{k_2 q_e^2} + \frac{t}{q_e}$	$q_{e,cal}$(mg/g)	42.23	67.02	43.16	125.0
	k_2(g/mg·h)	1.90×10^{-4}	8.42×10^{-5}	1.27×10^{-3}	1.26×10^{-4}
	R^2	0.6842	0.8054	0.9539	0.9837
$q_t = \alpha + \beta \ln t$	α(mg/g)	−49.29	−55.92	−5.54	−29.71
	β	18.16	20.89	9.283	21.58
	R^2	0.9322	0.9784	0.9553	0.8823

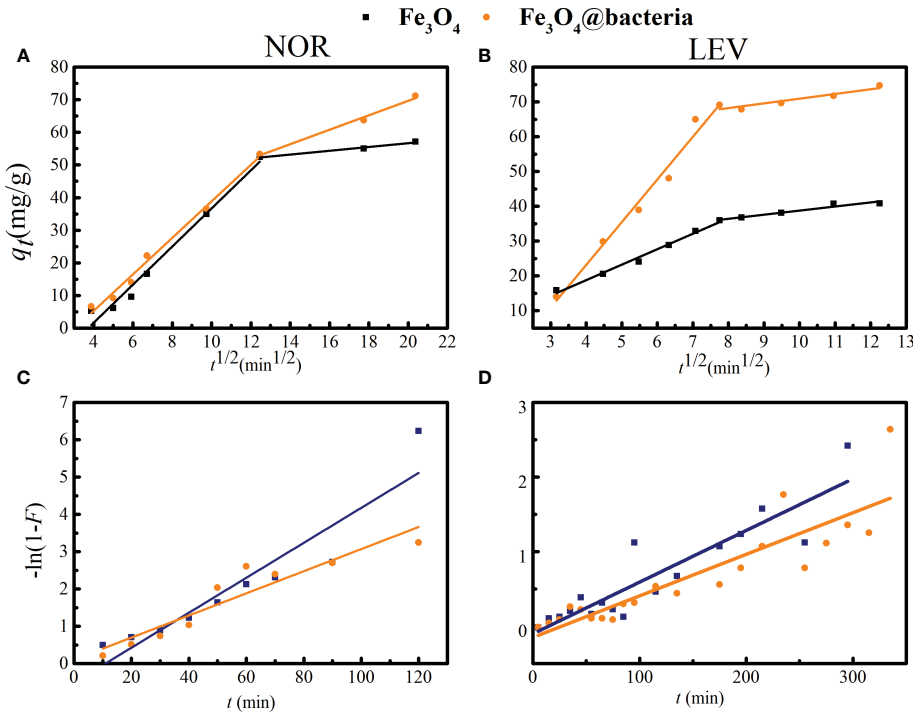

FIGURE 4
The particle diffusion model **(A ,B)** and LFD model **(C, D)** of norfloxacin (NOR) and levofloxacin (LEV) adsorption by Fe_3O_4 and a magnetic microrobot.

shows that chemisorption may have occurred. ΔS was positive, demonstrating that the solid/solution interface contains additional unpredictability. It might be connected to the fact that the molecules of the displaced solvent (like water) gained more translational energy than the molecules of the adsorbate lost (de Andrade et al., 2018).

To investigate the adsorption thermodynamics of NOR and LEV on magnetic microrobots, a range of temperatures, including 298, 303, 308, 313, and 318 K, were chosen. It can be seen in Table 5 that the ΔH of the adsorption of NOR was negative, demonstrating that both physical and chemical adsorption was involved in the exothermic process. For the LEV adsorption by a magnetic microrobot, it is an endothermic process (ΔH), which suggests that chemisorption may have occurred. Since ΔS was positive, the solid/solution interface must have had additional randomness. It could be related to the fact that the adsorbate molecules lost less translational energy than the displaced solvent molecules (like water) (de Andrade et al., 2018). $\Delta G < 0$, which means that adsorption was advantageous and spontaneous at any temperature.

3.6 Adsorption site energy analysis

Based on Equation (17), the equilibrium NOR and LEV adsorption capacities q_e are plotted as a function of the magnetic

TABLE 4 Adsorption kinetic models on norfloxacin (NOR) and levofloxacin (LEV) using Fe_3O_4 and a magnetic microrobot.

Kinetic model*	Parameters	NOR		LEV	
		Fe_3O_4	magnetic microrobot	Fe_3O_4	magnetic microrobot
LFD $-\ln(1-F) = k_3 t$	$K_3(\text{min}^{-1})$	0.00693	0.00557	0.04686	0.02966
	R^2	0.8200	0.7773	0.8649	0.8651
IPD $q_t = k_{IPD} t^{1/2} + c$	$k_1(\text{mg/g·min}^{1/2})$	5.84	5.60	4.44	12.27
	$c_1(\text{mg/g})$	−21.69	−17.11	1.04	−25.89
	R^2	0.9764	0.9882	0.9876	0.9790
	$k_1(\text{mg/g·min}^{1/2})$	0.58	2.21	27.00	57.41
	$c_2(\text{mg/g})$	45.06	24.40	1.18	1.35
	R^2	0.9670	0.9808	0.9264	0.8397

TABLE 5 Adsorption thermodynamic parameters of norfloxacin (NOR) and levofloxacin (LEV) adsorption by a magnetic microrobot.

Absorbent	ΔH (kJ/mol)	ΔS (J/(K·mol))	ΔG (kJ/mol)				
			293(K)	298(K)	303(K)	308(K)	313(K)
Fe_3O_4(NOR)	−67.01	−219.79	−2.58	−1.48	−0.38	0.72	1.82
magnetic microrobot (NOR)	−88.78	−291.42	−3.35	−1.89	−0.44	1.02	2.48
Fe_3O_4(LEV)	−7.36	−22.73	−0.36	−0.55	−0.54	−0.31	−0.25
magnetic microrobot (LEV)	20.25	66.64	0.71	0.38	0.05	−0.29	−0.62

microrobot's site energy E^* values in Figure 5. The E^* values decreased dramatically as the amount of NOR and LEV adsorbed on adsorbents increased. These findings demonstrated that NOR and LEV molecules occupied the magnetic microrobot's high-energy adsorption sites first, and then the low-energy adsorption sites. After the adsorbate occupied the high-energy sites, low-energy sorption sites interacted with the NOR and LEV molecules as the solution concentration rose. This was in line with the earlier NOR adsorption on carbon nanotubes (Wang et al., 2010). On a magnetic microrobot, the values of NOR's site energy E^* were significantly lower than those of LEV's. The E^* values of NOR adsorbed on the magnetic microrobot fell in the range of 4.25 to 10.73 kJ/mol, and the E^* values of LEV ranged from 17.36 to 21.22 kJ/mol. Additionally, the plots of E^* showed an increase with temperature, indicating that the NOR and LEV adsorption on the magnetic microrobot benefited from higher temperatures.

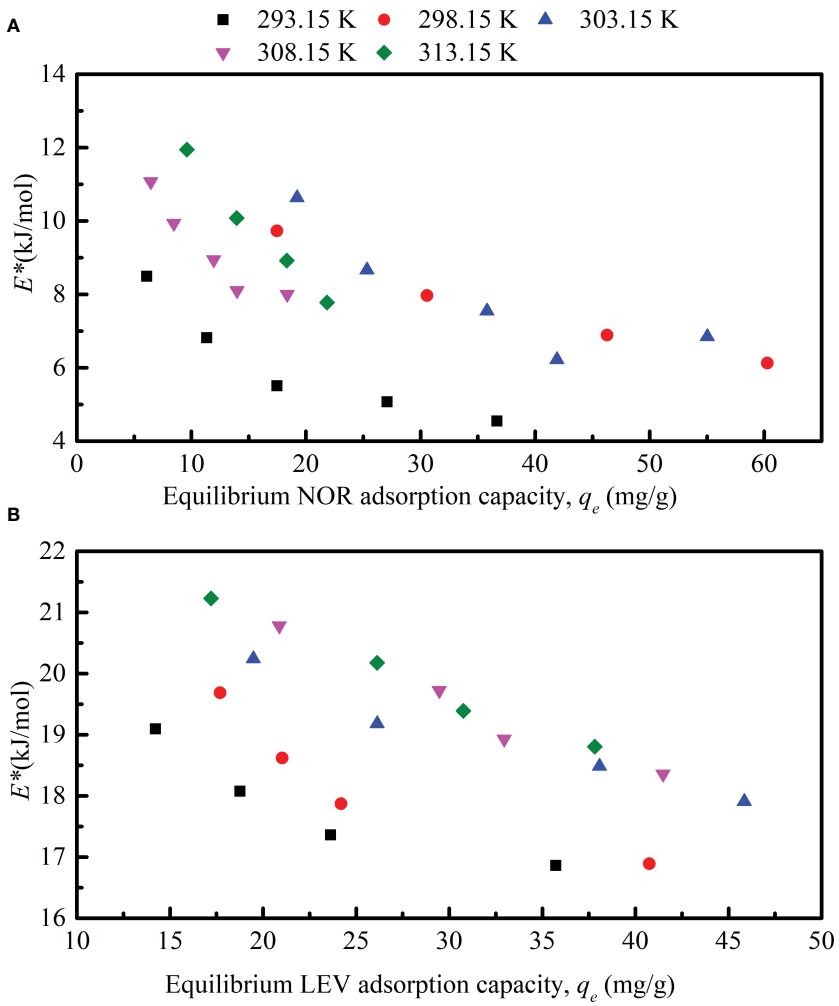

FIGURE 5
Site energy of norfloxacin (NOR) and levofloxacin (LEV) adsorption. **(A)** site energy versus equilibrium NOR adsorption capacity; **(B)** site energy versus equilibrium LEV adsorption capacity.

Temperature increased the rate of molecular diffusion, making it easier for NOR and LEV molecules to cross the magnetic microrobot's external boundary layer and enter its internal pores.

Based on the Langmuir–Freundlich isotherm model, the approximate site energy distribution ($F(E^*)$) for the adsorption of NOR and LEV to the magnetic microrobot at various temperatures is depicted in Figure 6. For NOR and LEV, the site energy had unimodal distributions. Most of the NOR and LEV sorption occurred on the sites with energy over 4.0 kJ/mol and lower than 16.0 kJ/mol, indicating that NOR and LEV sorption on the biosorbent was a physical-chemical process. First, as the site energy (E^*) increased, the frequency function $F(E^*)$ decreased until it was close to zero. The upward trend suggests that, at high concentrations, some NOR and LEV molecules were forced to occupy lower-energy sites. Conversely, at low-solution concentrations, NOR and LEV molecules were preferentially captured at the high-energy site (Zhang et al., 2021). Owing to the lower $F(E^*)$, however, the extremely high- or low- energy sites contributed very little to the maximum amount of adsorption (Liu et al., 2016).

4 Conclusion

The magnetic microrobot demonstrated outstanding NOR and LEV adsorption capacities. The static maximum adsorption capacities of NOR and LEV on the magnetic microrobot were 114.8 and 49.4 mg/g, respectively. The Langmuir isotherm model and Elovich kinetic models agreed well with the experimental data of NOR adsorption by a magnetic microrobot. The Langmuir isotherm model and the pseudo-second-order kinetic model might be able to adequately describe the LEV adsorption procedure. The IPD was not the only mechanism regulating the adsorption process, and the IPD model was better suited to describe the mass transfer process of the NOR and LEV adsorption by magnetic microrobot. Exothermic and spontaneous characteristics were verified through thermodynamics. The biosorbents' heterogeneous surface was verified by the analysis of site energy distribution. Additionally, Figure 6 demonstrated that the majority of the NOR and LEV adsorption took place on sites with greater than 4.25 kJ/mol and less than 17.36 kJ/mol, supporting the notion

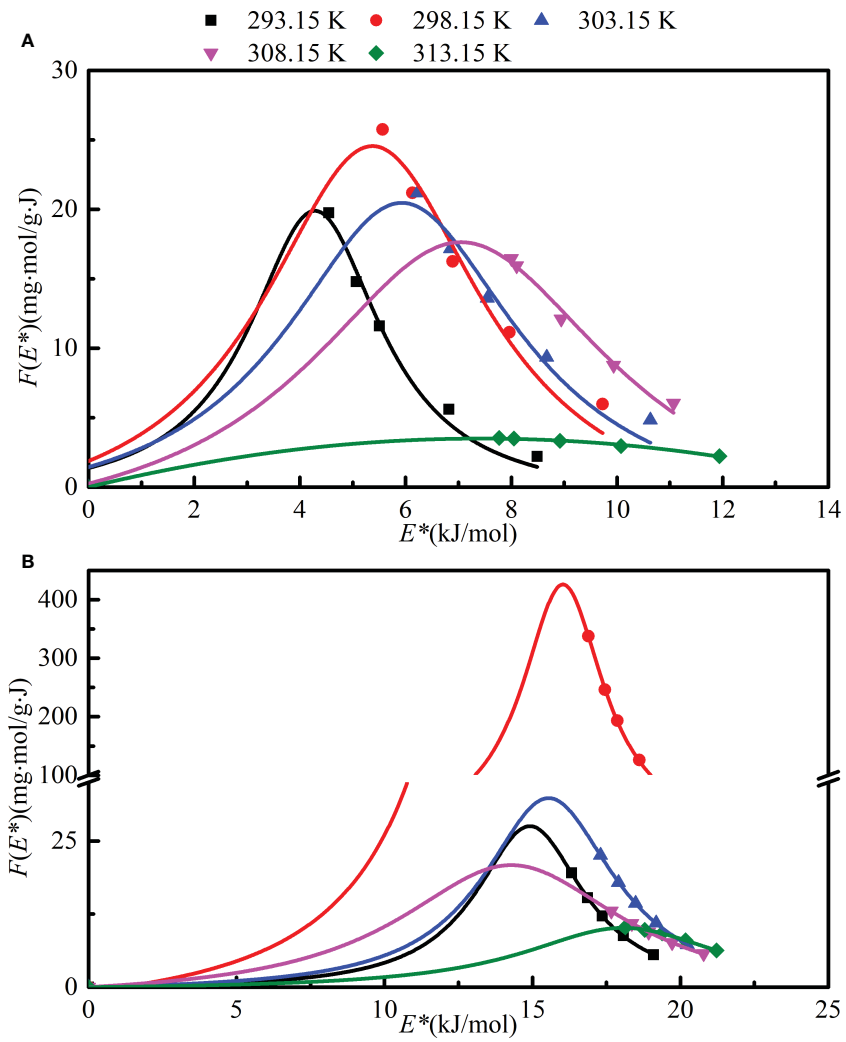

FIGURE 6
Site energy distribution of norfloxacin (NOR) and levofloxacin (LEV) adsorption on a magnetic microrobot at various temperatures. **(A)** Site energy distribution of NOR; **(B)** site energy distribution of LEV.

that this adsorption was physical–chemical in nature. Based on the findings, the magnetic microrobot can potentially be employed to inexpensively and efficiently remove NOR and LEV from aqueous wastewater as a new-style green bio-adsorbent.

Data availability statement

The original contributions presented in the study are included in the article/Supplementary Material. Further inquiries can be directed to the corresponding author.

Author contributions

YT: resources, funding acquisition, writing—reviewing and editing. WJ: investigation, methodology, and data handling. MB: writing—reviewing and editing. SQ: funding acquisition, writing—reviewing and editing. YP: conceptualization, resources, writing—reviewing and editing, supervision, funding acquisition. CL: investigation, methodology. JZ: methodology, resources, data handling. All authors contributed to the article and approved the submitted version.

Funding

This research was financially supported by the Shandong Provincial Natural Science Foundation (ZR2022QD018); the National Key R&D Program of China (2018YFD0900802); the National Innovation and Entrepreneurship Training Program for College Students (202111066013); the Yantai University Doctoral Start-up Foundation (HX2018B32); and the Shandong Key Laboratory of Marine Ecological Restoration (201919).

Conflict of interest

The authors declare that the research was conducted in the absence of any commercial or financial relationships that could be construed as a potential conflict of interest.

Publisher's note

Supplementary material

The Supplementary Material for this article can be found online at: https://www.frontiersin.org/articles/10.3389/fmars.2023.1169883/full#supplementary-material

References

Abukhadra, M. R., AlHammadi, A. A., Khim, J. S., Ajarem, J. S., and Allam, A. A. (2022). Enhanced decontamination of levofloxacin residuals from water using recycled glass based a green zinc oxide/mesoporous silica nanocomposite; adsorption and advanced oxidation studies. *J. Clean. Prod.* 356, 131836. doi: 10.1016/j.jclepro.2022.131836

Altaf, S., Zafar, R., Zaman, W. Q., Ahmad, S., Yaqoob, K., Syed, A., et al. (2021). Removal of levofloxacin from aqueous solution by green synthesized magnetite (Fe_3O_4) nanoparticles using *Moringa olifera*: kinetics and reaction mechanism analysis. *Ecotox. Environ. Safe.* 226, 112826. doi: 10.1016/j.ecoenv.2021.112826

Blokhina, S. V., Sharapova, A. V., Ol'khovich, M. V., Volkova, T. V., and Perlovich, G. L. (2016). Solubility, lipophilicity, and membrane permeability of some fluoroquinolone antimicrobials. *Eur. J. Pharm. Sci.* 93, 29–37. doi: 10.1016/j.ejps.2016.07.016

Carter, M. C., Kilduff, J. E., and Weber, W. J. (1995). Site energy distribution analysis of preloaded adsorbents. *Environ. Sci. Technol.* 29 (7), 1773–1780. doi: 10.1021/es00007a013

Chen, Z. X., Jin, X. Y., Chen, Z., Megharaj, M., and Naidu, R. (2011). Removal of methyl orange from aqueous solution using bentonite-supported nanoscale zero-valent iron. *J. Colloid. Interface Sci.* 363 (2), 601–607. doi: 10.1016/j.jcis.2011.07.057

Chen, Z., Ma, W., Lu, G., Meng, F., Duan, S., Zhang, Z., et al. (2019). Adsorption of levofloxacin onto mechanochemistry treated zeolite: modeling and site energy distribution analysis. *Sep. Purif. Technol.* 222, 30–34. doi: 10.1016/j.seppur.2019.04.010

Cheng, N., Wang, B., Wu, P., Lee, X., Xing, Y., Chen, M., et al. (2021). Adsorption of emerging contaminants from water and wastewater by modified biochar: a review. *Environ. pollut.* 273, 116448. doi: 10.1016/j.envpol.2021.116448

Chu, D., Dong, H., Li, Y., Xiao, J., Xiang, S., Dong, Q., et al. (2022). Insights into the correlation between different adsorption/oxidation/catalytic performance and physiochemical characteristics of fe-Mn oxide-based composites. *J. Hazard. Mater.* 439, 129631. doi: 10.1016/j.jhazmat.2022.129631

Coffie, E. S., Xie, L., Hassan, M., Shi, B., Ashraf, G. A., and Zhang, B. (2021). Energy-positive removal of norfloxacin in the bioelectro fenton system with nanoferrite-based composite electrodes. *Energ. Fuel.* 35, 4502–4511. doi: 10.1021/acs.energyfuels.0c04170

de Andrade, J. R., Oliveira, M. F., da Silva, M. G. C., and Vieira, M. G. A. (2018). Adsorption of pharmaceuticals from water and wastewater using nonconventional low-cost materials: a review. *Ind. Eng. Chem. Res.* 57, 3103–3127. doi: 10.1021/acs.iecr.7b05137

Fang, N., He, Q., Sheng, L., Xi, Y., Zhang, L., Liu, H., et al. (2021b). Toward broader applications of iron ore waste in pollution control: adsorption of norfloxacin. *J. Hazard. Mater.* 418, 126273. doi: 10.1016/j.jhazmat.2021.126273

Fang, L., Miao, Y. X., Wei, D., Zhang, Y., and Zhou, Y. C. (2021a). Efficient removal of norfloxacin in water using magnetic molecularly imprinted polymer. *Chemosphere* 262, 128032. doi: 10.1016/j.chemosphere.2020.128032

Foroutan, R., Peighambardoust, S. J., Peighambardoust, S. H., Pateiro, M., and Lorenzo, J. M. (2021). Adsorption of crystal violet dye using activated carbon of lemon wood and activated carbon/Fe_3O_4 magnetic nanocomposite from aqueous solutions: a kinetic, equilibrium and thermodynamic study. *Molecules* 26, 2241. doi: 10.3390/molecules26082241

Gaho, M. M., Zuhra Memon, G., Rehman Memon, J., Arain, J. B., Arain, A. J., Shah, A., et al. (2022). Synthesis of novel magnetic molecularly imprinted polymers by solid-phase extraction method for removal of norfloxacin. *Chin. J. Anal. Chem.* 50 (6), 100079. doi: 10.1016/j.cjac.2022.100079

Gao, Y., Guo, L., Jin, C., Zhao, Y., Gao, M., She, Z., et al. (2022). Metagenomics and network analysis elucidating the coordination between fermentative bacteria and microalgae in a novel bacterial-algal coupling reactor (BACR) for mariculture wastewater treatment. *Water Res.* 215, 118256. doi: 10.1016/j.watres.2022.118256

Hacıosmanoglu ˘, G. G., Mejías, C., Martín, J., Santos, J. L., Aparicio, I., and Alonso, E. (2022). Antibiotic adsorption by natural and modified clay minerals as designer adsorbents for wastewater treatment: a comprehensive review. *J. Environ. Manage.* 317, 115397. doi: 10.1016/j.jenvman.2022.115397

Ji, F., Wang, B., and Zhang, L. (2020). Light-triggered catalytic performance enhancement using magnetic nanomotor ensembles. *Research* 2020, 6380794. doi: 10.34133/2020/6380794

Jiang, W., Cui, W. R., Liang, R. P., and Qiu, J. D. (2021). Zwitterionic surface charge regulation in ionic covalent organic nanosheets: synergistic adsorption of fluoroquinolone antibiotics. *Chem. Eng. J.* 417, 128034. doi: 10.1016/j.cej.2020.128034

Jiang, F., Du, R., Yan, X., Zhang, M., Han, Q., Sun, X., et al. (2020). Ferroferric oxide nanoclusters decorated Ti_3C_2Tx nanosheets as high performance anode materials for lithium ion batteries. *Electrochim. Acta* 329, 135146. doi: 10.1016/j.electacta.2019.135146

Jiang, F., Liu, Y., Wang, Q., and Zhou, Y. (2018). Hierarchical Fe_3O_4@NC composites: ultralong cycle life anode materials for lithium-ion batteries. *J. Mater. Sci.* 53, 2127–2136. doi: 10.1007/s10853-017-1651-z

Kah, M., Sigmund, G., Xiao, F., and Hofmann, T. (2017). Sorption of ionizable and ionic organic compounds to biochar, activated carbon, and other carbonaceous materials. *Water Res.* 124, 673–692. doi: 10.1016/j.watres.2017.07.070

Lakshmi Prabavathi, S., and Muthuraj, V. (2019). Superior visible light driven photocatalytic degradation of fluoroquinolone drug norfloxacin over novel $NiWO_4$ nanorods anchored on g-C_3N_4 nanosheets. *Colloid. Surface. A. Physicochem. Eng. Asp.* 567, 43–54. doi: 10.1016/j.colsurfa.2019.01.040

Li, C., Gao, Y., Li, A., Zhang, L., Ji, G., Zhu, K., et al. (2019a). Synergistic effects of anionic surfactants on adsorption of norfloxacin by magnetic biochar derived from furfural residue. *Environ. Pollut.* 254, 113005. doi: 10.1016/j.envpol.2019.113005

Li, J., Ji, F., Ng, D. H. L., Liu, J., Bing, X., and Wang, P. (2019b). Bioinspired pt-free molecularly imprinted hydrogel-based magnetic janus micromotors for temperature-responsive recognition and adsorption of erythromycin in water. *Chem. Eng. J.* 369, 611–620. doi: 10.1016/j.cej.2019.03.101

Liu, Y., Dong, C., Wei, H., Yuan, W., and Li, K. (2015). Adsorption of levofloxacin onto an iron-pillared montmorillonite (clay mineral): kinetics, equilibrium and mechanism. *Appl. Clay. Sci.* 118, 301–307. doi: 10.1016/j.clay.2015.10.010

Liu, J., Li, J., Wang, G., Yang, W., Yang, J., and Liu, Y. (2019). Bioinspired zeolitic imidazolate framework (ZIF-8) magnetic micromotors for highly efficient removal of organic pollutants from water. *J. Colloid. Interface Sci.* 555, 234–244. doi: 10.1016/j.jcis.2019.07.059

Liu, F. F., Zhao, J., Wang, S., and Xing, B. (2016). Adsorption of sulfonamides on reduced graphene oxides as affected by pH and dissolved organic matter. *Environ. pollut.* 210, 85–93. doi: 10.1016/j.envpol.2015.11.053

Lv, X., Yan, D. Y. S., Lam, F. L. Y., Ng, Y. H., Yin, S., and An, A. K. (2020). Solvothermal synthesis of copper-doped BiOBr microflowers with enhanced adsorption and visible-light driven photocatalytic degradation of norfloxacin. *Chem. Eng. J.* 401, 126012. doi: 10.1016/j.cej.2020.126012

Nguyen, V. T., Vo, T. D. H., Nguyen, T. B., Dat, N. D., Huu, B. T., Nguyen, X. C., et al. (2022). Adsorption of norfloxacin from aqueous solution on biochar derived from spent coffee ground: master variables and response surface method optimized adsorption process. *Chemosphere* 288, 132577. doi: 10.1016/j.chemosphere.2021.132577

Oberoi, A. S., Jia, Y., Zhang, H., Khanal, S. K., and Lu, H. (2019). Insights into the fate and removal of antibiotics in engineered biological treatment systems: a critical review. *Environ. Sci. Technol.* 53, 7234–7264. doi: 10.1021/acs.est.9b01131

Patel, M., Kumar, R., Kishor, K., Mlsna, T., Pittman, C. U., and Mohan, D. (2019). Pharmaceuticals of emerging concern in aquatic systems: chemistry, occurrence, effects, and removal methods. *Chem. Rev.* 119, 3510–3673. doi: 10.1021/acs.chemrev.8b00299

Pi, Y. R., Bao, M. T., Li, Y. M., Li, G. M., Lu, J. R., and Sun, P. Y. (2015). Characterization of crude oil degrading microbial cultures isolated in qingdao China. *RSC. Adv.* 5 (118), 97665–97674. doi: 10.1039/C5RA16628D

Pi, Y., Duan, C., Zhou, Y., Sun, S., Yin, Z., Zhang, H., et al. (2022). The effective removal of Congo red using a bio-nanocluster: Fe_3O_4 nanoclusters modified bacteria. *J. Hazard. Mater.* 424, 127577. doi: 10.1016/j.jhazmat.2021.127577

Rai, P. K., Sonne, C., Brown, R. J. C., Younis, S. A., and Kim, K. (2022). Adsorption of environmental contaminants on micro- and nano-scale plastic polymers and the influence of weathering processes on their adsorptive attributes. *J. Hazard. Mater.* 427, 127903. doi: 10.1016/j.jhazmat.2021.127903

Rezaei, F., and Vione, D. (2018). Effect of pH on zero valent iron performance in heterogeneous fenton and fenton-like processes: a review. *Molecules* 23, 3127. doi: 10.3390/molecules23123127

Ross, D. L., and Riley, C. M. (1990). Aqueous solubilities of some variously substituted quinolone antimicrobials. *Int. J. Pharm.* 63 (3), 237–250. doi: 10.1016/0378-5173(90)90130-V

Sarmah, A. K., Meyer, M. T., and Boxall, A. B. (2006). A global perspective on the use, sales, exposure pathways, occurrence, fate and effects of veterinary antibiotics (VAs) in the environment. *Chemosphere* 65, 725–759. doi: 10.1016/j.chemosphere.2006.03.026

Saya, L., Malik, V., Gautam, D., Gambhir, G., Balendra,, Singh, W. R., et al. (2022). A comprehensive review on recent advances toward sequestration of levofloxacin antibiotic from wastewater. *Sci. Total. Environ.* 813 (2022), 152529. doi: 10.1016/j.scitotenv.2021.152529

Scaria, J., Gopinath, A., Ranjith, N., Ravindran, V., Ummar, S., Nidheesh, P. V., et al. (2022). Carbonaceous materials as effective adsorbents and catalysts for the removal of emerging contaminants from water. *J. Clean. Prod.* 350, 131319. doi: 10.1016/j.jclepro.2022.131319

Schwertmann, U., and Cornell, R. M. (2000). *Iron oxides in the laboratory: preparation and characterization. 2nd ed.* (New York, USA: Wiley-VCH).

Singh, A. K., Bhuyan, T., Maity, S., Mandal, T. K., and Bandyopadhyay, D. (2020). Magnetically actuated carbon soot nano-particle-based catalytic CARBOts coated with Ni/Pt nanofilms for water detoxification and oil-spill recovery. *ACS Appl. Nano. Mater.* 3, 3459–3470. doi: 10.1021/acsanm.0c00199

Sun, M., Yang, Y., Huang, M., Fu, S., Hao, Y., Hu, S., et al. (2022). Adsorption behaviors and mechanisms of antibiotic norfloxacin on degradable and nondegradable microplastics. *Sci. Total. Environ.* 807, 151042. doi: 10.1016/j.scitotenv.2021.151042

Vaghasiya, J. V., Mayorga-Martinez, C. C., Matějková, S., and Pumera, M. (2022). Pick up and dispose of pollutants from water *via* temperature-responsive micellar copolymers on magnetite nanorobots. *Nat. Commun.* 13, 1026. doi: 10.1038/s41467-022-28406-5

Van Doorslaer, X., Dewulf, J., Van Langenhove, H., and Demeestere, K. (2014). Fluoroquinolone antibiotics: an emerging class of environmental micropollutants. *Sci. Total. Environ.* 500, 250–269. doi: 10.1016/j.scitotenv.2014.08.075

Wammer, K. H., Korte, A. R., Lundeen, R. A., Sundberg, J. E., McNeill, K., and Arnold, W. A. (2013). Direct photochemistry of three fluoroquinolone antibacterials norfloxacin, ofloxacin, and enrofloxacin. *Water Res.* 47, 439–448. doi: 10.1016/j.watres.2012.10.025

Wan, Y., Liu, X., Liu, P., Zhao, L., and Zou, W. (2018). Optimization adsorption of norfloxacin onto polydopamine microspheres from aqueous solution: kinetic, equilibrium and adsorption mechanism studies. *Sci. Total. Environ.* 639, 428–437. doi: 10.1016/j.scitotenv.2018.05.171

Wang, X., Lin, Y., Zheng, Y., and Meng, F. (2022). Antibiotics in mariculture systems: a review of occurrence, environmental behavior, and ecological effects. *Environ. pollut.* 293, 118541. doi: 10.1016/j.envpol.2021.118541

Wang, A., Liu, C., Ge, X., Meng, W., Pi, Y., and Liu, C. (2021). Enhanced removal of Congo red dye from aqueous solution by surface modified activated carbon with bacteria. *J. Appl. Microbiol.* 131, 2270–2279. doi: 10.1111/jam.15100

Wang, X., Yin, R., Zeng, L., and Zhu, M. (2019a). A review of graphene-based nanomaterials for removal of antibiotics from aqueous environments. *Environ. Pollut.* 253, 100–110. doi: 10.1016/j.envpol.2019.06.067

Wang, J., Zhang, M., Zhou, R., Li, J., Zhao, W., and Zhou, J. (2020). Adsorption characteristics and mechanism of norfloxacin in water by γ-Fe_2O_3@BC. *Water Sci. Technol.* 82, 242–254. doi: 10.2166/wst.2020.078

Wang, D., Zhao, G., Chen, C., Zhang, H., Duan, R., Zhang, D., et al. (2019b). One-step fabrication of dual optically/magnetically modulated walnut-like micromotor. *Langmuir* 35, 2801–2807. doi: 10.1021/acs.langmuir.8b02904

Wang, Z. Y., Yu, X. D., Pan, B., and Xing, B. S. (2010). Norfloxacin sorption and its thermodynamics on surface-modified carbon nanotubes. *Environ. Sci. Technol.* 44 (3), 978–984. doi: 10.1021/es902775u

Xu, Z., Xiang, Y., Zhou, H., Yang, J., He, Y., Zhu, Z., et al. (2021). Manganese ferrite modified biochar from vinasse for enhanced adsorption of levofloxacin: effects and mechanisms. *Environ. pollut.* 272, 115968. doi: 10.1016/j.envpol.2020.115968

Yan, B., and Niu, C. H. (2017). Modeling and site energy distribution analysis of levofloxacin sorption by biosorbents. *Chem. Eng. J.* 307, 631–642. doi: 10.1016/j.cej.2016.08.065

Yan, B., and Niu, C. H. (2018). Adsorption behavior of norfloxacin and site energy distribution based on the dubinin - astakhov isotherm. *Sci. Total. Environ.* 631-632, 1525–1533. doi: 10.1016/j.scitotenv.2018.03.119

Yan, B., Niu, C. H., and Wang, J. (2017a). Kinetics, electron-donor-acceptor interactions, and site energy distribution analyses of norfloxacin adsorption on pretreated barley straw. *Chem. Eng. J.* 330, 1211–1221. doi: 10.1016/j.cej.2017.08.056

Yan, B., Niu, C. H., and Wang, J. (2017b). Analyses of levofloxacin adsorption on pretreated barley straw with respect to temperature: kinetics, π-π electron-donor-acceptor interaction and site energy distribution. *Environ. Sci. Technol.* 51, 8048–8056. doi: 10.1021/acs.est.7b00327

Yang, Q., Gao, Y., Ke, J., Show, P. L., Ge, Y., Liu, Y., et al. (2021). Antibiotics: an overview on the environmental occurrence, toxicity, degradation, and removal methods. *Bioengineered* 12 (1), 7376–7416. doi: 10.1080/21655979.2021.1974657

Yang, D., Li, J., Luo, L., Deng, R., He, Q., and Chen, Y. (2020). Exceptional levofloxacin removal using biochar-derived porous carbon sheets: mechanisms and density-functional-theory calculation. *Chem. Eng. J.* 387, 124103. doi: 10.1016/j.cej.2020.124103

Yao, B., Luo, Z., Du, S., Yang, J., Zhi, D., and Zhou, Y. (2021). Sustainable biochar/$MgFe_2O_4$ adsorbent for levofloxacin removal: adsorption performances and mechanisms. *Bioresour. Technol.* 340, 125698. doi: 10.1016/j.biortech.2021.125698

Yu, J., Zhang, X., Jin, B., Chen, J., Huang, Y., and Wang, Z. (2021). Silica aluminum xerogel-based sorbent for removal of volatilized $PbCl_2$ during the incineration: improvement on mass-transfer limitations *via* high porosity. *Sci. Total. Environ.* 782, 146925. doi: 10.1016/j.scitotenv.2021.146925

Zhang, X., Chu, Y., Zhang, H., Hu, J., Wu, F., Wu, X., et al. (2021). A mechanistic study on removal efficiency of four antibiotics by animal and plant origin precursors-derived biochars. *Sci. Total. Environ.* 772, 145468. doi: 10.1016/j.scitotenv.2021.145468

Zhang, Y., Yan, K., Ji, F., and Zhang, L. (2018). Enhanced removal of toxic heavy metals using swarming biohybrid adsorbents. *Adv. Funct. Mater.* 28, 1806340. doi: 10.1002/adfm.201806340

Zhou, L., Li, N., Owens, G., and Chen, Z. (2019). Simultaneous removal of mixed contaminants, copper and norfloxacin, from aqueous solution by ZIF-8. *Chem. Eng. J.* 362, 628–637. doi: 10.1016/j.cej.2019.01.068

Zhou, H., Mayorga-Martinez, C. C., Pané, S., Zhang, L., and Pumera, M. (2021). Magnetically driven micro and nanorobots. *Chem. Rev.* 121, 4999–5041. doi: 10.1021/acs.chemrev.0c01234

Zhou, H., Wang, Z., Gao, C., Sun, Q., Liu, J., and She, D. (2023). Synthesis of honeycomb lignin-based biochar and its high-efficiency adsorption of norfloxacin. *Bioresour. Technol.* 369, 128402. doi: 10.1016/j.biortech.2022.128402

Zhou, A., Zhu, C., Chen, W., Wan, J., Tao, T., Zhang, T. C., et al. (2018). Phosphorus recovery from water by lanthanum hydroxide embedded interpenetrating network poly (vinyl alcohol)/sodium alginate hydrogel beads. *Colloids. Surf. A. Physicochem. Eng. Asp.* 554, 237–244. doi: 10.1016/j.colsurfa.2018.05.086